Reprinted from

MATERIALS SCIENCE & ENGINEERING A

Materials Science and Engineering A209 (1996) 277–286

Tribological properties of AlN-CeO_2-Si_3N_4 cutting materials in unlubricated sliding against tool steel and cast iron

J.R. Gomes[a], A.S. Miranda[a], R.F. Silva[b], J.M. Vieira[b]

[a] *Departamento de Engenharia Mecânica, Universidade do Minho, 4800 Guimarães, Portugal*
[b] *Departamento de Engenharia Cerâmica e do Vidro, Universidade de Aveiro, 3800 Aveiro, Portugal*

ELSEVIER

ELSEVIER

Materials Science and Engineering A209 (1996) 277–286

MATERIALS SCIENCE & ENGINEERING A

Tribological properties of AlN-CeO_2-Si_3N_4 cutting materials in unlubricated sliding against tool steel and cast iron

J.R. Gomes[a], A.S. Miranda[a], R.F. Silva[b], J.M. Vieira[b]

[a]*Departamento de Engenharia Mecânica, Universidade do Minho, 4800 Guimarães, Portugal*
[b]*Departamento de Engenharia Cerâmica e do Vidro, Universidade de Aveiro, 3800 Aveiro, Portugal*

Abstract

Ceramic pins of the AlN-CeO_2-Si_3N_4 system were tested in a pin-on-disc tribometer against discs of tool steel and grey cast iron, at room temperature, without lubrication, in different conditions of humidity and sliding speed. Ceramic samples were selected on the basis of their mechanical properties (hardness and fracture toughness), and microstructural characteristics, namely porosity, volume of intergranular phase and nitrogen content of the glass phase.

Water vapour increased the weight loss of the nitride by promoting the tribo-oxidation wear mode and by weakening the adhesion of debris to the ceramic surfaces. In dry air, the adhering wear debris provided protection to the sliding surfaces and the wear coefficients of the ceramic converged to similar values for tests with both iron alloys. For the ceramic/tool steel tribopairs, the ceramic surfaces become more protected as the amount of the intergranular glassy layer of the nitride is increased, as the glassy phase gives enhanced debris adhesion. Microcracking of the ceramic surface was the dominant wear mode and the volumic wear rate was found to be dependent on the inverse of hardness and fracture toughness. In humid environments, the effect of roughness of the grey cast iron worn surface surmounted the dependence of the wear rate on microstructural and mechanical properties of the nitride, which was found in the ceramic/steel tribopairs.

The sliding speed has a strong effect on the wear behaviour. At low speeds, no protective plates of debris were detected on the worn surfaces. When the speed was increased above 0.5 ms^{-1}, the wear coefficient values fell down almost one order of magnitude. The wear coefficients of porous nitride materials of relative open porosity close to 20%, tested against cast iron, were unexpectedly lower than the values obtained for dense materials of same composition ($K \approx 2 \times 10^{-15}$ Pa^{-1} for porous samples and $K \approx 1.5 \times 10^{-14}$ Pa^{-1}, for fully dense samples). SEM observations showed an extensive coating by the metallic rich debris, that performed a solid lubricant action.

Keywords: Tribological properties; Ceramics

1. Introduction

Silicon nitride ceramics are potential candidates for machine triboelements for application under extreme conditions, such as those found in reciprocating engines, wear parts and cutting tools [1–4]. Ceramics are generally harder and more wear resistant than metals in corrosive environments at high temperatures. Data on silicon nitride/iron alloys tribopairs [2,5–11] are comparatively sparse compared with data on the wear characteristics of Si_3N_4 self-mated pairs [3,4,12–19]. However, these studies show that moisture adsorption and sliding speed have a major influence on the friction and wear behaviour of nitride ceramics. The wear rate is usually larger at high humidity but, when the sliding speed is increased, the contact surface becomes dry owing to frictional heating. The increase of the wear coefficient of Si_3N_4 with moisture was explained by corrosion effects [3] or weakening of adhesion of the oxidized wear particles to the ceramic surface [8]. Both Si_3N_4/steel and Si_3N_4/grey cast iron experiments result in high wear coefficients ($K \approx 10^{-14}$ Pa^{-1}), and high friction coefficients ($f \approx 0.8$). No systematic comparison has yet been performed between the wear behaviour of Si_3N_4 against the two iron alloys.

SSDI 0921-5093(95)10154-3

Papers on the influence of microstructural properties of silicon nitride materials on their tribological behaviour are also rare [20]. However, the following effects were reported [20]: (i) the Hall–Petch relation between grain size and wear resistance is observed; (ii) grains of rounded shapes are low stress concentrators compared with angular ceramic grains; (iii) pores can either work as stress concentrators or can blunt the crack fronts; (iv) the role of the intergranular phase is contradictory: segregated impurities weak the grain boundaries and increase the mechanical wear, on the reverse case, an amorphous grain boundary phase can enhance creep flow and improves the wear resistance [20].

In this study, the rare earth oxide CeO_2 was chosen as the sintering aid for Si_3N_4 owing to its chemical resistance [21] and it provides the increase in the sintering rate [22] and the viscosity of the oxynitride glassy, intergranular layer [22]. Tool steel and grey cast iron were studied as counterface materials because these alloys are potential workpiece materials in cutting [1]. Wear mechanisms of Si_3N_4 depend on microstructural characteristics such as the amount and composition of the intergranular phase, α-Si_3N_4 content and porosity, and also on the mechanical properties such as hardness and fracture toughness of the ceramic. The effects of relative humidity in the range 2%–98%RH and of sliding speeds on the wear rate of Si_3N_4 at constant values of load are further investigated.

2. Experimental details

2.1. Materials

Different ceramic materials of the system AlN-CeO_2-Si_3N_4 were selected on the basis of their hardness, H, fracture toughness, K_{Ic}, N-content and microstructural features such as porosity, P, and volume of the intergranular glass phase, V_L. The ceramic pins were machined from discs that were hot-pressed in the temperature range of 1350–1650 °C at 30 MPa. Chemical composition, nitrogen content and volume fraction of intergranular glassy phase for three grades of low (LA), medium (MA) and high (HA) additive content of the samples, are given in Table 1. Volume fraction of the intergranular phase, V_L, and its N-content were calculated from the amount and composition of the sintering aids, using densities of glasses of similar composition [22].

Samples with open porosity close to 20% were hot pressed at 1350 °C. Higher temperatures resulted in nearly complete densification of the remaining samples, Table 2. As the temperature increases, grain growth and α-$Si_3N_4 \rightarrow \beta$-$Si_3N_4$ phase transformation are enhanced, thus resulting in the H and K_{Ic} values presented in Table 2. The hardness was measured using a Vicker indenter with a load of 9.8 N, and taking an averag from 20 indentations for each sample. For each inden tation, the Palmqvist-type crack lengths were measure and the fracture toughness was determined according t Niihara et al.'s expression [23]. The α-Si_3N_4 weigh fraction was calculated from the peak heights of th X-ray diffraction patterns using the calibration metho of Gazzara and Messier [24].

Table 1
Composition of Si_3N_4-based materials and intergranular phas volume

Batch	Composition (mol. %)				V_L (%)	N (at.%)
	Si_3N_4	SiO_2	Ce_2O_3	AlN		
LA	76.2	7.3	0.9	15.6	10.1	27.1
MA	73.2	7.5	1.8	17.5	12.6	26.3
HA	69.0	8.0	3.5	19.5	16.9	24.2

Raw materials: Si_3N_4, H.C. Starck LC12; CeO_2, Fluka grade puris AlN, H.C. Starck grade C.

Tool steel (TS) and grey cast iron (GCI) were used a counterface disc materials. The composition and prop erties of the two alloys are given in Table 3. The surfac of the discs was polished with 800 grit silicon carbid paper followed by finishing with 1 μm diamond paste and ultrasonically degreased with ethanol. Surfac roughnesses of the polished surfaces, as measured b profilometry, were 0.05 μm and 0.3 μm Ra for stee and cast iron, respectively.

2.2. Testing procedure

Non-lubricated friction and wear tests were carrie out in a conventional pin-on-disc tribometer. The ex periments were conducted inside an acrylic chamber fo isolation from the ambient environment. High relativ humidity environments (98%RH) were obtained b blowing air through a water reservoir of controlle

Table 2
Hot pressing temperatures and microstructural and mechanical prop erties of the ceramic samples

Designation	T (°C)	Relative density (%)	α-Si_3N_4 (w.%)	H (GPa)	K_{Ic} (MPam$^{1/2}$)
LA-1	1500	98.9	61.4	19.7	4.1
LA-2	1550	99.7	50.3	19.5	4.2
LA-3	1600	99.8	38.3	19.0	4.7
LA-4	1650	99.8	26.3	18.2	5.2
MA-P	1350	80.7	92.3	5.4	–
MA-D	1450	96.9	85.3	18.2	4.1
HA-P	1350	84.4	89.4	6.2	–
HA-D	1450	99.7	89.8	17.9	3.5

Table 3
Properties of tool steel and cast iron discs

Material	Code	Composition	H (GPa)
Annealed Tool Steel (TS)	DIN 1.2080	2.0%C; 12%Cr	2.5
Grey Cast Iron (GCI)	Grade 200	3.9%C; 2.9%Si; 0.9%Mn; 0.04%(max)S; 0.1%(max)P	1.9

temperature. Low humidity conditions (2%RH) were obtained by using silica gel desiccant in the air circuit before the chamber inlet. Humidity was measured using a digital hygrometer.

A data acquisition system was used to record the frictional forces developed in the interface between the stationary pin and the rotating disc. The frictional force is proportional to the output signal of a bending-type loadcell which counteracted the pin holder displacement.

Pin-on-disc tests were stopped at regular time intervals and the weight loss of the pin was measured using a microbalance with an accuracy of 10 μg. The wear volume of the pin was calculated from the weight loss and the density of the material and the wear volume of the disc was measured by profilometry [1]. The friction coefficient and wear coefficient were evaluated at normal applied load, F_n, of 5 N. After an initial running-in, the sliding couple entered a steady state regime where the wear volume, V, became proportional to the sliding distance, x. The friction coefficient, f, is the ratio between the frictional force, F_f, and the normal load, $f = F_f/F_n$, the wear coefficient, K, is given by $K = V/(F_n \cdot x)$.

The wear surface of the pins and the wear tracks on the discs were periodically observed by optical microscopy, during the tests. At the end of each test, the worn surfaces of the pins, the wear debris, and the track surface of the discs were examined by analytical scanning electron microscopy (SEM) with EDS X-ray analysis.

Table 4
Friction coefficient, f, and pin wear coefficient, K_P (10^{-15} Pa^{-1}), for Si_3N_4 pins in different humidity conditions ($v = 0.5$ ms^{-1}, $F_n = 5$ N)

Material		RH = 2%		RH = 50%		RH = 98%	
Pin	Disc	f	K_P	f	K_P	f	K_P
LA	TS	0.81	3.3	0.77	11.0	0.89	12.0
MA	TS	0.93	6.2	0.78	7.5	0.90	14.0
HA	TS	0.70	4.1	0.72	8.7	0.83	8.7
LA	GCI	0.74	4.3	0.77	18.0	0.74	15.0
MA	GCI	0.83	4.1	0.73	15.0	0.87	19.0
HA	GCI	0.85	4.3	0.74	15.0	0.98	19.0

3. Results

3.1. Si_3N_4/tool steel contacts

Table 4 presents the experimental values of f, the friction coefficient, and, K_P, the pin wear coefficient, for the three ceramic grades in different humidity environments. K_P increases by 2–3 times for ceramic/TS contacts when the water vapour content of the test atmosphere is increased from 2%RH up to 50%RH and stabilises at high values in more humid environments. Fig. 1 is a plotting of K_P vs. the volume of the intergranular phase of the ceramics, V_L. In dry air, K_P is almost independent on this microstructural feature, while in humid air, RH $\geqslant$ 50%, K_P decreases with V_L.

Extensive layers of iron-rich wear debris are adherent to the ceramic surfaces when tested in dry air against TS (Fig. 2(a)). Under humid conditions, the adherent particles are less abundant and fine grooving of the ceramic surface is observed (Fig. 2(b)). For all test conditions, the morphology of the loose wear debris is a combination of large plates (10 μm) and fine particles (Fig. 2(c)). EDS analysis revealed that the particles are all composites of Si–Fe oxides.

The effect of changing the amount of intergranular phase on the wear behaviour was also investigated in the sliding speed range 0.05–3.5 ms^{-1} at RH = 50%.

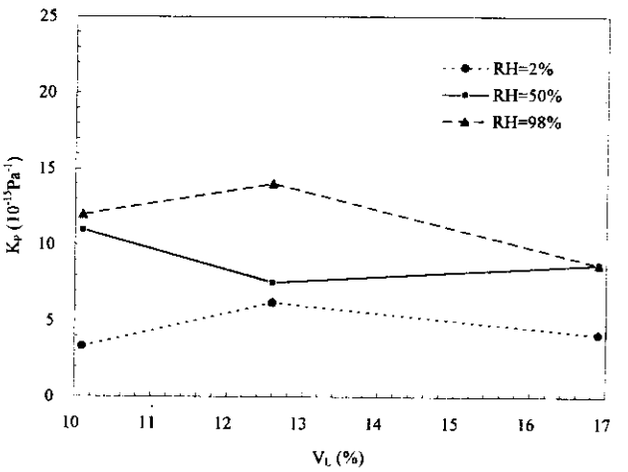

Fig. 1. Variation in the wear coefficient of Si_3N_4, K_P, with the volume of intergranular phase, V_L, in different humidity environments, against tool steel (TS).

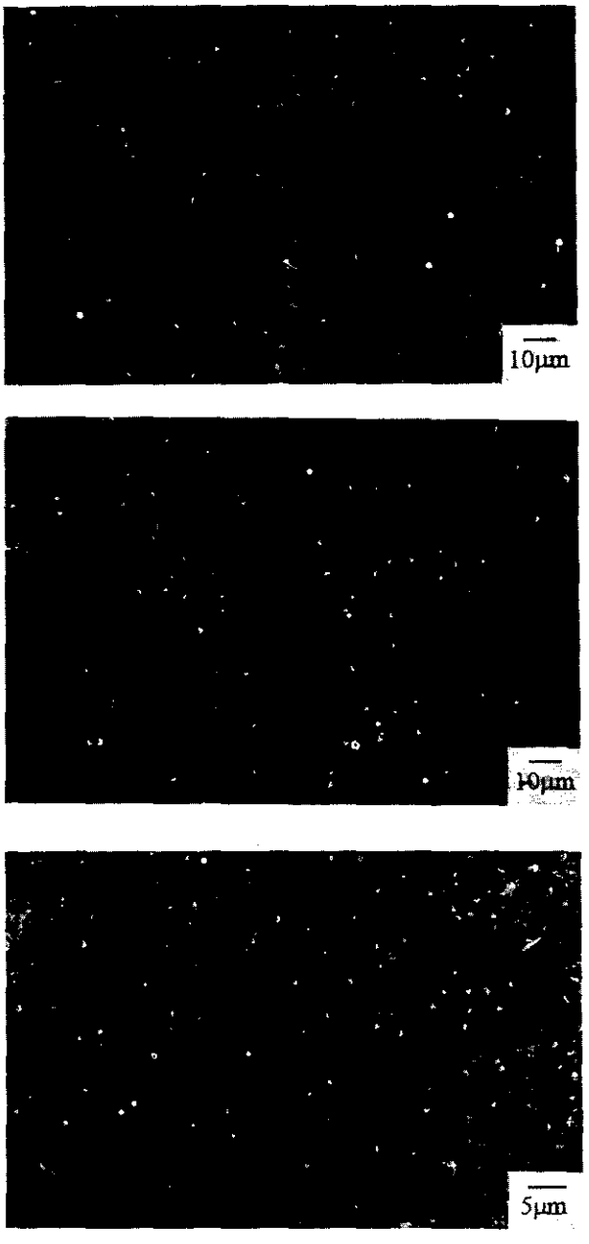

Fig. 2. Secondary electron images (SEM/SE) of the Si_3N_4 worn surfaces and wear debris tested in different humidity conditions against TS. (a) LA worn surface at RH = 2%; (b) LA worn surface at RH = 50%; (c) appearance of the loose wear debris.

Friction coefficients exhibited values between 0.72 and 0.85 without any correlation with the sliding speed. Changes in the pin wear coefficient for the LA and HA grades are shown in Fig. 3. K_P is lower for the HA material than for the LA material at low to medium speeds, while the opposite behaviour is observed above 0.5 ms^{-1}. These two regimes are characterised by quite different morphologies of the mating TS surfaces. In the low speed regime, the TS discs (Fig. 4(a)) and the ceramic pins (Fig. 2(b)) are almost free of adhering debris. In the high speed regime, the worn tracks on the TS discs show extensive plastic deformation (Fig. 4(b)). The ceramic surfaces in the high speed regime are partially coated with iron-rich plates (Fig. 4(c)).

The friction coefficient, and the pin wear coefficient for a set of dense samples of the LA Si_3N_4 grade are listed in Table 5. These samples were chosen in order to evaluate the dependence of K_P on hardness, H, and fracture toughness, K_{Ic}, when the microstructural characteristics, V_L, and porosity, and the experimental conditions of relative humidity, sliding speed, and normal applied load are held constant. For Si_3N_4/TS contacts K_P decreases with increasing K_{Ic} even though hardness is diminishing.

The tribological behaviour of porous and dense samples of two grades of Si_3N_4 was compared. The results for the friction and wear coefficients are given in Table 6, where K_D is the disc wear coefficient. For the TS contacts, the pin wear of the porous samples, MA-P and HA-P, is very high, with a catastrophic value ($K > 10^{-13}$ Pa^{-1}) for the ceramic of the highest intergranular glass content, HA-P. Disc wear in the Si_3N_4/TS system also increased in testing against the porous ceramics. The surfaces of the porous ceramics are fully covered with an iron-rich layer (Fig. 5(a)) as the result of intense metal removal from the TS surface (Fig. 5(b)). Representative EDS analysis of the worn surfaces of porous and dense Si_3N_4 materials are shown in Fig. 6(a) and (b), respectively. The EDS spectrum of the sliding surface of a dense sample (Fig. 6(b)), reveals the elements Si, Ce, Al, O, N corresponding to the original composition of the ceramic, while a high Fe-peak is noticed in the EDS spectrum of the worn surface of the porous ceramic (Fig. 6(a)), the Fe peak coming from the metallic-rich deposits reported above.

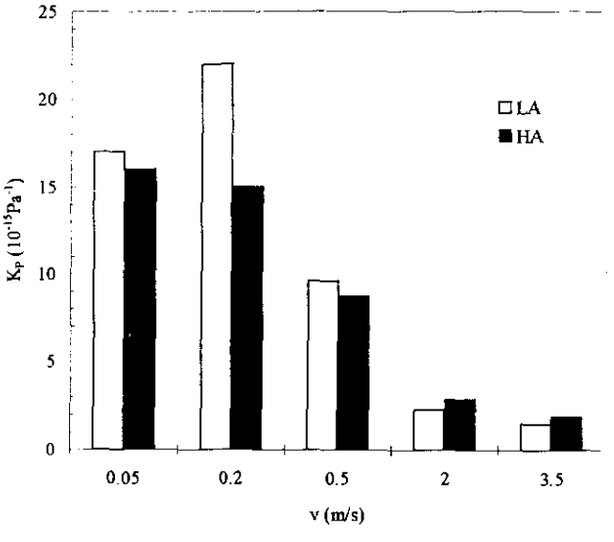

Fig. 3. Dependence of pin wear coefficient on the sliding speed for low (LA) and high (HA) additive content Si_3N_4 tested against TS

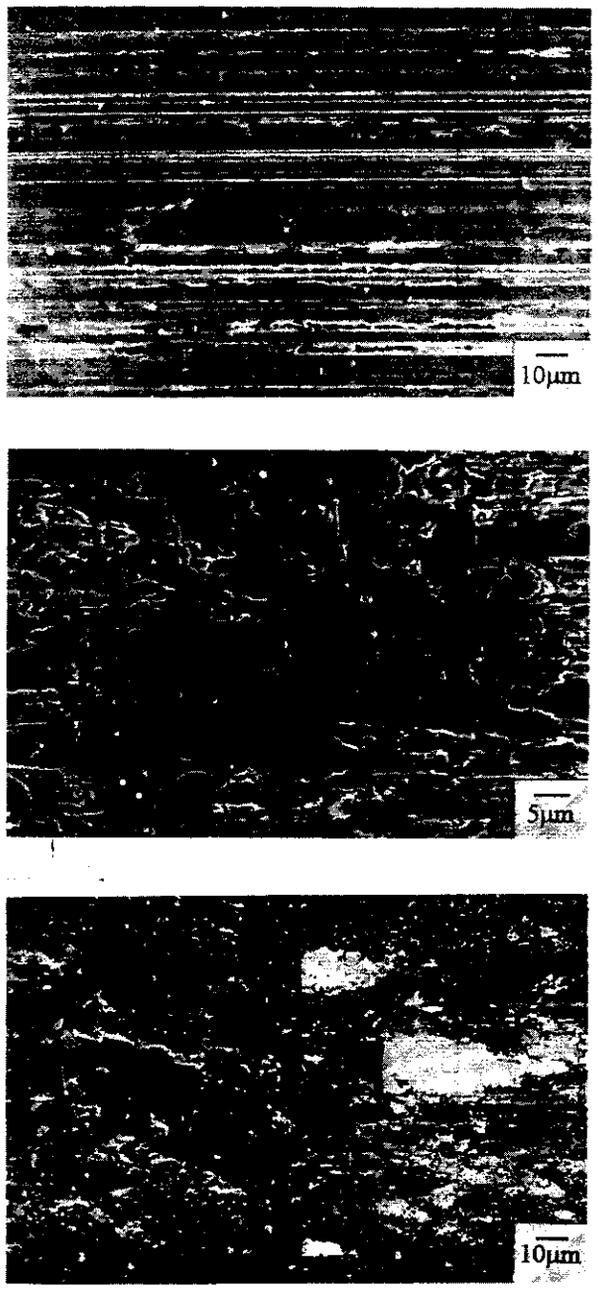

Fig. 4. SEM images of the ceramic pin and TS disc wear tracks tested at different sliding speeds; (a) TS disc surface after testing at $v = 0.05$ ms^{-1}; (b) TS disc surface at $v = 3.5$ ms^{-1}; (c) LA worn surface at $v = 3.5$ ms^{-1} (left, SEM/SE; right, SEM/BS micrographs).

3.2. Si_3N_4/grey cast iron contacts

The wear coefficient K_P for the ceramic/GCI contacts increases 3–4 times from dry air (2%RH) to 50%RH (Table 4). No changes in K_P were observed when humidity was further increased up to 98%RH. For each of the three environments K_P remain almost independent of the intergranular volume phase content of the ceramics, V_L (Fig. 7). As for the Si_3N_4/TS contacts in dry air (Fig. 2(a)) the ceramic pins were also covered by smeared iron-rich layers (Fig. 8(a)). In humid conditions, only few adherent wear debris can be seen on the ceramic surface, with smooth appearance (Fig. 8(b)). The loose wear debris (Fig. 8(c)) has large plates of Si–Fe oxides, some of them with lengths above 50 μm.

Table 5
Friction coefficient, f, and wear coefficient, K_P (10^{-15} Pa^{-1}), of LA-Si_3N_4 pins of different hardness and fracture toughness ($v = 0.5$ ms^{-1}, $F_n = 5$ N, RH = 50%)

	H	K_{Ic}	Ceramic/TS		Ceramic/GCI	
Sample	(GPa)	(MPam$^{1/2}$)	f	K_P	f	K_P
LA-1	19.7	4.1	0.77	11.0	0.77	18.0
LA-2	19.5	4.2	0.78	12.0	0.86	19.0
LA-3	19.0	4.7	0.73	9.6	0.81	18.0
LA-4	18.2	5.2	0.79	6.5	0.77	20.0

The dependence of K_P on V_L over the sliding speed range 0.05–3.5 ms^{-1}, was also studied against GCI as it was for TS alloy. K_P values (Fig. 9) reveal the same two regimes as a function of speed that were previously identified for the Si_3N_4/TS contacts (Fig. 3). At low speeds both surfaces, the ceramic pins (Fig. 8(b)) and the GCI discs (Fig. 10(a)) are poorly covered by wear debris. A characteristic feature of the high speed wear regime is the covering of the graphite flake cavities on the GCI wear track by material displaced in the sliding direction (Fig. 10(b)), while at very low speeds, the surface of GCI remains preserved and retains the polished appearance (Fig. 10(a)). At high speeds, 3.5 ms^{-1}, iron-rich plates partially coat the Si_3N_4 pin surface (Fig. 10(c)).

An odd result was obtained for porous samples of Si_3N_4 with the wear coefficient, K_P, one order of magnitude lower than the corresponding value for the dense Si_3N_4 samples. The effect is observed both in the Si_3N_4 materials of low and high V_L contents. The friction coefficients of those tribopairs are also the lowest among all the sets of experiments (Table 6). The porous ceramic pins were protected by an extensive layer of adherent debris (Fig. 11(a)). The GCI counterface disc also preserved the polishing appearence (Fig. 11(b)).

Table 6
Friction coefficient, f, and wear coefficients, K_P and K_D (10^{-15} Pa^{-1}), for Si_3N_4-based pins of different porosity ($v = 0.5$ ms^{-1}, $F_n = 5$ N, RH = 50%)

	Relative	Ceramic/TS			Ceramic/GCI		
Sample	porosity (%)	f	K_P	K_D	f	K_P	K_D
MA-P	19.3	0.78	34.5	20.0	0.50	1.8	4.6
HA-P	15.6	0.64	140.0	97.0	0.59	5.6	9.4
MA-D	3.1	0.78	7.5	1.5	0.73	15.0	4.5
HA-D	0.3	0.72	8.7	3.8	0.74	15.0	4.7

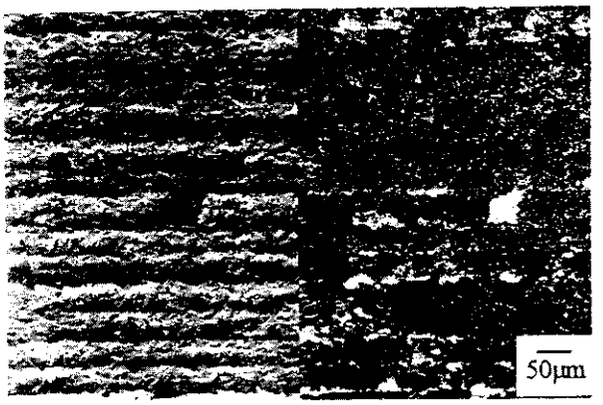

Fig. 5. Worn surfaces of the porous Si_3N_4 pin/TS wear experiments; (a) SEM/SE (left) and SEM/BS (right) micrographs of the MA-porous sample (MA-P); (b) wear track on TS disc from the MA-P/TS test (SEM/SE).

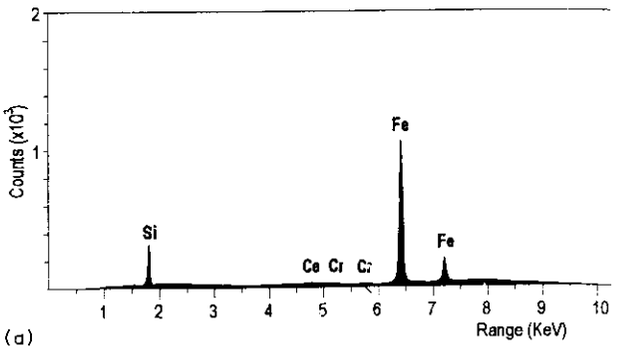

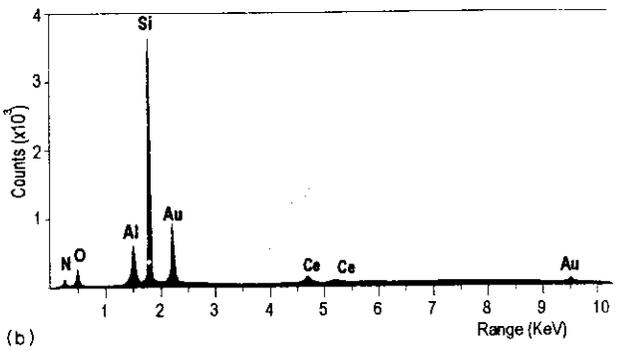

Fig. 6. SEM-EDS spectra of the worn Si_3N_4 surface after slidi against TS; (a) porous ceramic (MA-P); (b) dense sample (MA-D

4. Discussion

4.1. Effect of humidity and sliding speed on wear

The results of wear of Si_3N_4 against both iron alloys, TS and GCI, show similar dependence on humidity and sliding speed as plotted in Figs. 1, 3, 7 and 9, which are highlighted in the following.

In humid air (RH $\geqslant$ 50%), the wear behaviour of the Si_3N_4 pins for the TS contacts is dependent on the volume fraction of the intergranular phase, V_L (Fig. 1). Pin-on-disc contacts are "open-type", with an overlap ratio $\epsilon \ll 1$ for the disc, giving room for a strong interaction between the adsorbed gaseous species of the atmosphere and the contact interface [16]. Thus a marked effect of moisture results. Humidity increases the weight loss of ceramics not only by assisting the tribo oxidation wear mode [11], but also by changing the rheology of the wear debris and weakening the adhesion of debris to the ceramic surface [8,13,25]. As a result, the ceramic surfaces in humid environments show few aggregates of adherent wear debris when tested against both iron alloys (Figs. 2(b) and 8(b)). The reactivity of the Si–Fe oxidized wear particles with the glassy phase as well as the adhesion efficiency ar improved with V_L [1], thus leading to better surfac protection and low K_P.

In dry air, RH = 2%, the wear coefficients are muc lower (Table 4 and Figs. 1 and 7). The wear debr spreads on the ceramic pin surfaces in the slidin direction (Fig. 2(a) and Fig. 8(a)), performing "thir

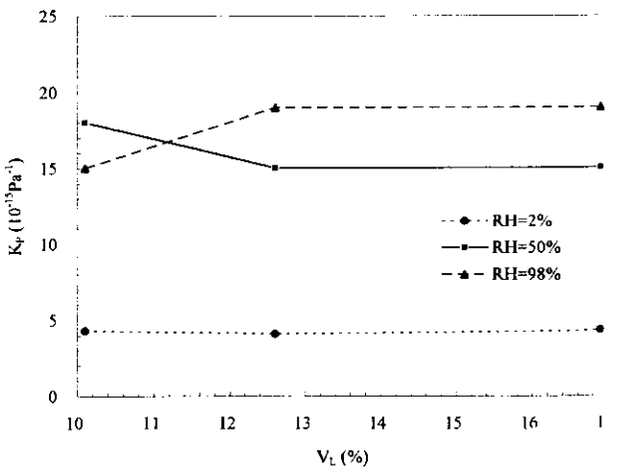

Fig. 7. Variation in the wear coefficient of Si_3N_4, K_P, with t volume of intergranular phase, V_L, in different humidity enviro ments, against grey cast iron (GCI).

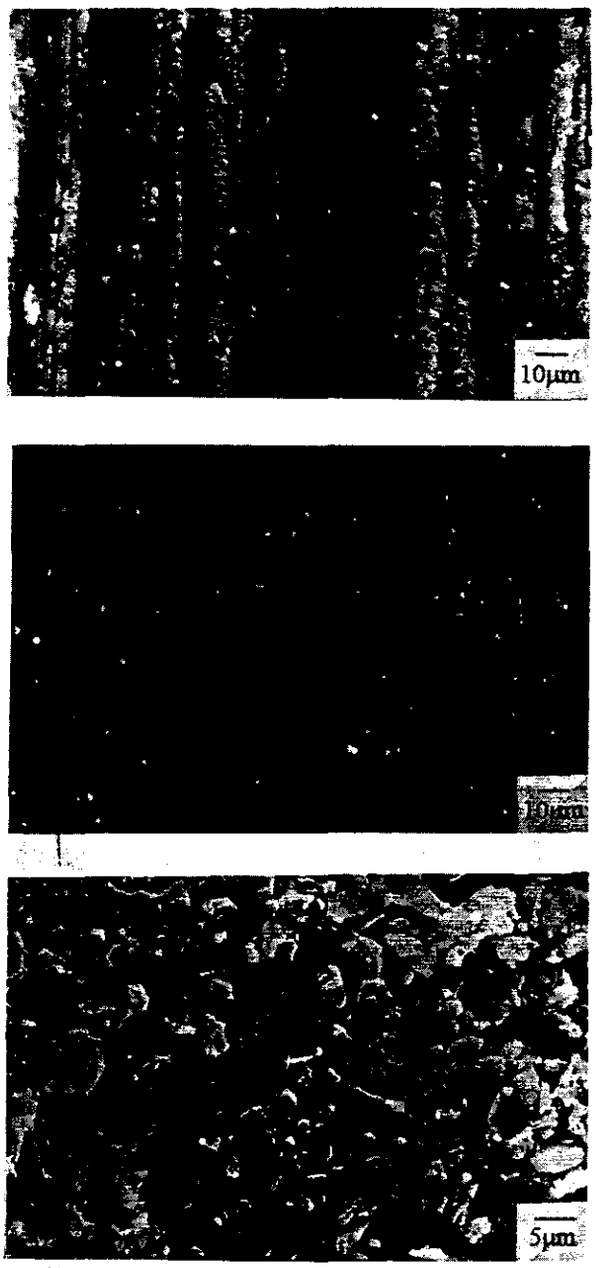

Fig. 8. Secondary electron images (SEM/SE) of the Si_3N_4 worn surfaces and wear debris tested in different humidity conditions against GCI (a) LA worn surface at RH = 2%; (b) LA worn surface at RH = 50%; (c) appearance of the loose wear debris.

body" protection [26]. All the wear coefficients tend to similar values when working against either TS or GCI (Figs. 1 and 7). When such protection is not operating, as described for humid conditions, the wear coefficient becomes very sensitive to the topography of the counterface [10] leading to higher wear coefficients against GCI than against TS (Figs. 1 and 7). GCI materials are more brittle than TS steel and its surface rougher. Under the influence of sliding and attendant heat generation, graphite is removed, creating large cavities in the track of the GCI disc. The severity of contact in the ceramic/GCI sliding couples increases with surface roughness [19,27] resulting in high contact stresses [10]. The mechanical wear is characterised by flake formation [19,27], the morphology of the loose debris found in these tests (Fig. 8(c)). The effect of roughness in the ceramic/GCI tribopairs, overcomes the dependence of wear on the intergranular glass amount, reported above for the TS contacts, where the severity was less and wear was characterised by formation of powder-like particles [19,27] (Fig. 2(c)). Graphite from the cast iron is reported to enhance the tribological performance of ceramic/GCI tribopairs [2], but if the surfaces are rough owing to pull out of the graphite, then the solid lubrication effect is seemingly secondary.

The sliding speed has a net effect on the wear behaviour of both ceramic grades. K_P decreases an order of magnitude for sliding speeds from 0.05 ms^{-1} to 3.5 ms^{-1} (Figs. 3 and 9). Two regimes can be distinguished: the sliding speed ranges below and above 0.5 ms^{-1}.

In the low speed regime, the contact conditions are of non-protective type, which is illustrated by the SEM images from the ceramic pins and metallic discs (Figs. 2(b), 8(b), 4(a) and 10(a)), the worn surfaces being almost free of wear agglomerates. In this regime, high additive (HA) Si_3N_4 materials show a better performance than the LA samples as a result of higher debris/glass contact area, as shown before. Fig. 4(a) shows a micrograph of the TS topography at low sliding speeds, which is almost a replica of the ceramic counterface morphology (Fig. 2(b)). This is a characteristic feature of surfaces with low debris accumulation.

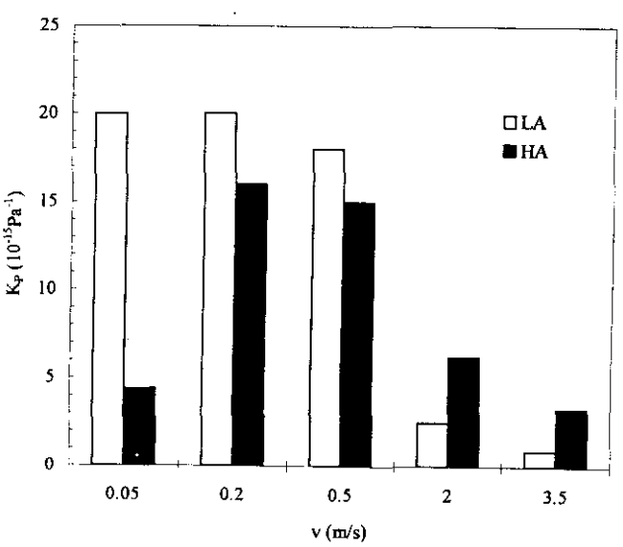

Fig. 9. Dependence of pin wear coefficient on the sliding speed for low (LA) and high (HA) additive content Si_3N_4 ceramics tested against GCI.

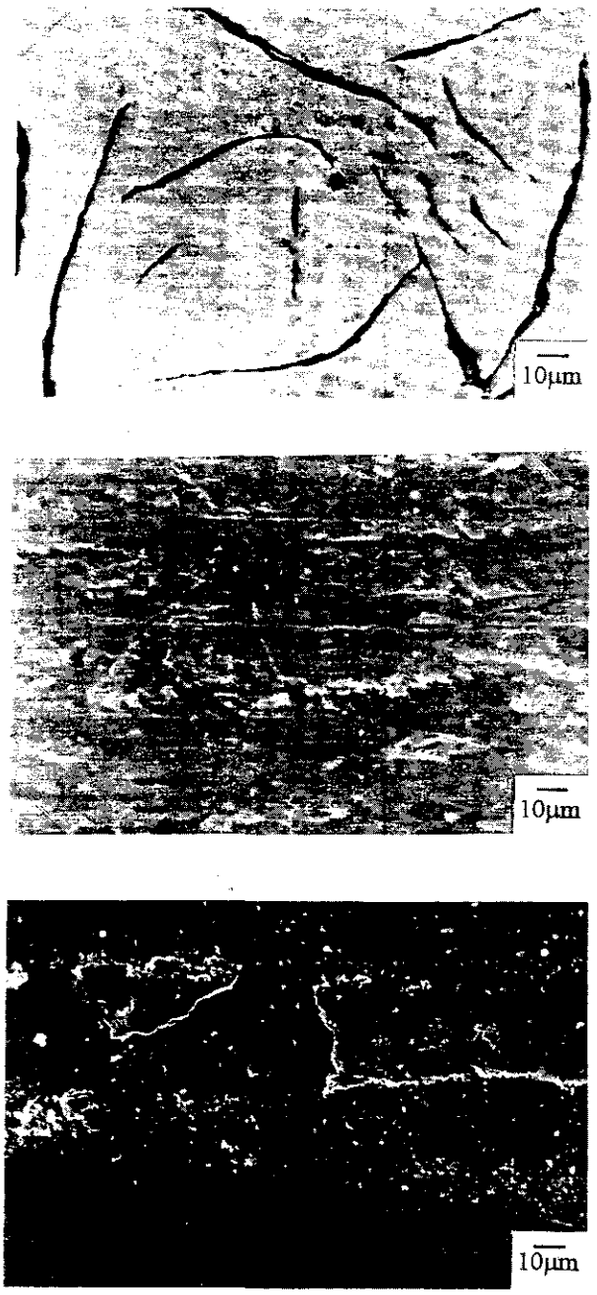

Fig. 10. SEM/SE images of the ceramic pin and GCI disc wear tracks tested at different sliding speeds; (a) GCI disc surface after testing at $v = 0.05$ ms^{-1}; (b) TS disc surface at $v = 3.5$ ms^{-1}; (c) LA worn surface at $v = 3.5$ ms^{-1}.

At high speed, the wear debris spreads on the ceramic surface leading to protection and to decreasing of the wear coefficient. High temperatures (flash temperatures) that are developed [3,5,28] result in extensive plastic deformation of the metal surfaces (Figs. 4(b) and 10(b)), and the metal is transferred to the ceramic counterface. The decrease in hardness of both materials, which is far steeper for the metal alloy, together with desorbtion of chemisorbed water molecules, were also reported as mechanisms contributing to enhancement of wear resistance of the ceramic [3]. The ceramic surfaces of both ceramic/TS and ceramic/GCI contacts tend to be similarly covered (Figs. 4(c) and 10(c)) and the wear coefficients of the pins are considerably lower, and the difference between the two sets of data decreases (Figs. 3 and 7). For the high speed regime, the dependence on the amount of intergranular glass is the opposite of the one observed in the low speed regime; the HA nitride wearing more than the LA grade. As heat is developed in the ceramic/metal contact at high sliding speeds, the wear resistance of the ceramic becomes a function of the thermomechanical properties, namely the hot hardness [29]. Hot hardness of silicon nitride ceramics decreases with V_L and with low N content of the glasses [22,29]. The HA grade presents at the same time the highest V_L and the lowest N-content, Table 1, thus bringing lower wear resistance to this ceramic material at high sliding speeds.

4.2. Surface microcracking in Si_3N_4/tool steel sliding pairs

Influence of the mechanical properties of the nitride samples is implicit in the dependence of the ceramic

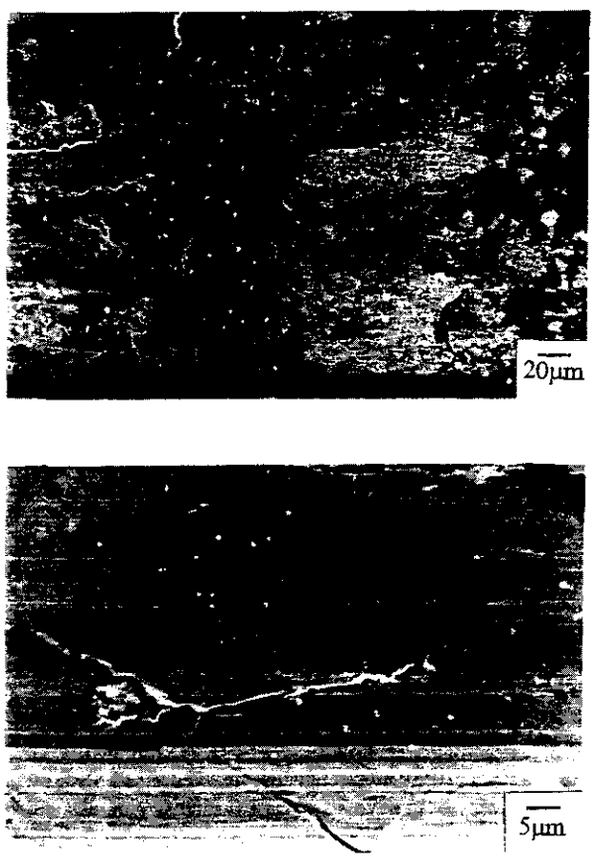

Fig. 11. Worn surfaces of the porous pin/GCI wear experiments; (a) SEM/SE (left) and SEM/BS (right) micrographs of the MA-porous sample (MA-P); (b) wear track on GCI disc from the MA-P/GCI test (SEM/SE).

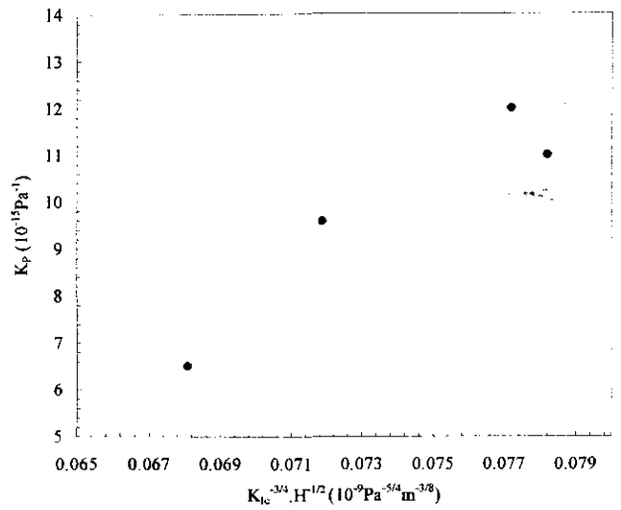

Fig. 12. Plotting of the dependence of the wear coefficient on the fracture toughness (K_{Ic}) and hardness (H) for the LA nitrides tested against tool steel, according to the abrasive wear model.

tribological behaviour on intergranular phase volume and porosity discussed above. These microstructural properties are held constant in the set of LA samples 1–4 in Table 2, but the amounts of α/β-Si_3N_4 phase differ, thus resulting in distinct H, K_{Ic}, and wear coefficient values (Table 5). For those conditions where the surface of the ceramic pin is not protected by an adherent "third-body" layer, as found in the present study for tests at medium speed, in humid environments, the mechanical wear mode must become the main mechanism of wear [19,27]. For the ceramic/TS sliding contacts, the powder-formation mode by surface microcracking was the dominant mode of wear. The corresponding wear coefficient, K, which is directly proportional to the volume of removed material, is given by $K = A\ H^{-1/2}\ K_{Ic}^{-3/4}$ [30], A being a constant that is dependent on the normal load (F_n) and on the sliding distance (x) [30]. The linear correlation in Fig. 12, where this equation is used, corroborates that abrasion of the Si_3N_4 ceramic materials, is dependent on the coupled values of the two mechanical properties, H and K_{Ic} [31]. The abrasive wear mode is the result of sliding indentation actions from the loose ceramic grains [5] or the chromium carbide hard particles coming from the tool steel. When large, flake-like wear particles are formed, which occurred when the nitride samples were tested against the rougher GCI material (Fig. 8(c)), the brittle fracture threshold of the ceramic surface has a complex dependence on its mechanical properties [19,27,30]. For the range of H and K_{Ic} of the samples the wear coefficients of the dense nitride pins against GCI are almost constant (Table 5) and no correlation could be found with these mechanical properties.

4.3. Self protection in porous Si_3N_4/grey cast iron sliding pairs

As expected, porosity of the Si_3N_4 samples has a remarkable effect on the tribological behaviour of Si_3N_4. However, opposite trends were observed for tests against TS and GCI. While the K_P values of the porous samples against the tool steel are very high, the same materials show low values of K_P for the ceramic/GCI tribopairs (Table 6). Observation of representative morphologies of the worn pin surfaces reveals extensive spreading of metallic-rich debris for both type of alloys (Figs. 5(a) and 11(a)). However, this layer had a protective action in the ceramic/GCI contact for both the nitride and the grey cast iron since the beginning of the sliding motion, whereas in the ceramics/TS pair it was the result of great amounts of wear debris coming from the TS metal that was extensively worn (Fig. 5(b)). This is corroborated by the plots of the friction coefficient over the first 1000 m of sliding distance for porous and dense ceramics sliding against the iron alloys (Fig. 13). For the MA-P/TS couple, the friction coefficient rises almost instantaneously to its maximum value and remains stationary throughout the run. The increases of the friction force is very sharp and the high wear regime is early attained. Microfracture of the porous ceramic material produces a rough contact surface, which increases the stresses and further enhances fracture. In this severe wear regime, the metallic disc also undergoes high wear (Table 6), and a considerable amount of wear debris is formed, which accumulates on the pin counterface. In the MA-D/TS sliding couple, the stationary friction regime is also quickly reached, but at low values of f, K_P and K_D, and only after a larger sliding distance (x). The wear coefficients of both triboelements, pin and disc, are lower. The initial topography

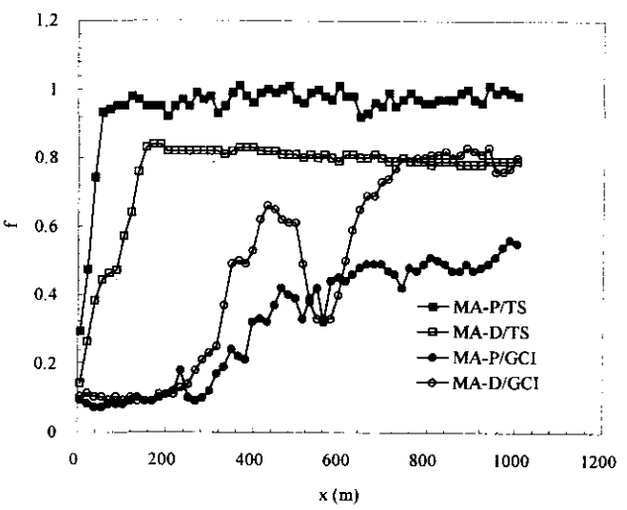

Fig. 13. Initial values of the friction coefficient as a function of sliding distance for porous (MA-P) and dense (MA-D) Si_3N_4 samples.

of both surfaces is well preserved due to the high mechanical resistance of the dense nitride [20].

Friction grows slowly in the MA-P/GCI sliding pair (Fig. 13) as the result of the progressive coating of the ceramic surface by the metallic layer, with graphite providing lubrication characteristics (Fig. 11(a)). The pores and cavities of the porous ceramic surface retain most of the metallic debris (Fig. 11(a)). On the contrary, the worn surface of the dense nitride, tested under the same conditions, is smoother (Fig. 8(b)) and adhesion of the wear debris is weaker. The result is a higher friction coefficient for the dense ceramic/GCI pair (MA-D/GCI), coupled with increasing wear (Table 6). After a short distance, the friction force rises to the steady state level that overlaps with the corresponding values of the MA-D/TS sliding (Fig. 13). The low friction coefficient of the MA-P/GCI sliding pair, $f \approx 0.5$ (Table 6), contributes to low disc wear coefficient of GCI and to preservation of its original surface when sliding against the porous nitride (Fig. 11(b)).

5. Conclusions

Large differences in wear behaviour of CeO_2-AlN-Si_3N_4 ceramics are observed when steel or grey cast iron are used as counterface materials. Grey cast iron surfaces are rougher due to graphite pull-out. Cavities resulting from graphite flake depletion lead to severe contact. The effect of roughness overcomes the dependence of the wear coefficient on the intergranular phase content of the Si_3N_4 and its composition that was found in the case of the tool steel contacts. In the latter contacts, the adhesion of the Si–Fe oxidized wear debris to the ceramic surface increases with the amount of sintering aid in Si_3N_4, resulting in a protective coating of the ceramic surface. A dependence of the wear coefficient, K, on the surface microcraking model, $K \propto H^{-1/2}$. $K_{Ic}{}^{-3/4}$, was also found for the ceramic/steel contacts.

Humidity and sliding speed have opposite trends on the wear resistance of the nitrides. The wear coefficient increases with relative humidity due to the lack of debris adhesion. Increasing the sliding speed results in frictional heating and extensive smearing of the wear debris over the ceramic surface, as a consequence of drying of the tribo contact. In the speed regime above 0.5 ms^{-1}, the wear resistance of the ceramics becomes a function of the thermomechanical properties which decrease with the volumic fraction of the intergranular glass and with the reduction of its N-content.

When Si_3N_4 ceramics with 20% porosity were tested against cast iron, surprisingly they wore one order of magnitude less than a dense Si_3N_4 ceramic of the same composition. The corresponding friction coefficient also showed the lowest value of all experiments ($f \approx 0.5$). A lubricating graphite wear debris layer that strongly adhered to the porous ceramic surface is claimed to be the cause of such positive performance.

References

[1] R. Silva, J. Gomes, A. Miranda and J. Vieira, *Wear, 148* (1991) 69–89.
[2] L. Fang, Y. Gao, L. Zhou and P. Li, *Wear, 171* (1994) 129–134.
[3] K.H. Lee and K.W. Kim, *Mater. Sci. Eng., A186* (1994) 185–191.
[4] H.E. Sliney and C. Dellacorte, *J. Soc. Tribologists and Lubrication. Eng., 50*(7) (1994) 571–576.
[5] M.F. Wani, J. Mukerji, B. Prakash and S. Bandopadhyay, *Am Ceram. Soc. Bull., 72*(9) (1993) 82–87.
[6] L. Zhou, L. Fang, N.X. Wang and J.E. Zhou, *Tribology Int., 27*(5) (1994) 349–357.
[7] P. Andersson and K. Holmberg, *Wear, 175* (1994) 1–8.
[8] M.G. Gee and D. Butterfield, *Wear, 162–164* (1993) 234–245.
[9] J. Conway, R. Pangborn, P. Cohen and D. Love, *Wear, 126* (1988) 79–90.
[10] J.K. Lancaster, Y. A-H. Mashal and A.G. Atkins, *J. Phys. D: Appl. Phys., 25* (1992) A205–A211.
[11] H. Czichos, S. Becker and J. Lexow, *Wear, 135* (1989) 171–191.
[12] A. Zutshi, R.A. Haber, D.E. Niesz, J.W. Adams, J.B. Wachtman, M.K. Ferber and S.M. Hsu, *J. Am. Ceram. Soc., 77*(4) (1994) 883–890.
[13] T.E. Fischer, H. Liang and W.M. Mullins, *Mater. Res. Symp. Proc., 140* (1989) 339–342.
[14] X. Dong and S. Jahanmir, *Wear, 165* (1993) 169–180.
[15] A. Blomberg, M. Olsson, J. Brathäll and S. Hogmark, *Proc. Int. Tribol. Conf.*, Brisbane, 1990, pp. 79–84.
[16] A. Skoop, M. Woydt and K.-H. Habig, *Tribology Int., 23*(3) (1990) 189–199.
[17] J. Denape and J. Lamon, *J. Mater. Sci., 25* (1990) 3592–3604.
[18] S. Sasaki, *Wear, 134* (1989) 185–200.
[19] K. Kato, *Wear, 136* (1990) 117–133.
[20] B. Gueroult and K. Cherif, *J. Canadian Ceram. Soc., 63*(2) (1994) 132–142.
[21] S.T. Buljan and S.F. Wayne, *Adv. Ceram. Mater., 2*(4) (1987) 813–816.
[22] R.F. Silva, A.P. Moreira, J.M. Gomes, A.S. Miranda and J.M. Vieira, *Mater. Sci. Eng., A168* (1993) 55–59.
[23] K. Niihara, R. Morena and D.P. Hasselman, *J. Mater. Sci. Lett., 1* (1982) 13–16.
[24] C.P. Gazzara and D.R. Messier, *Am. Ceram. Soc. Bull., 56*(9) (1977) 777–780.
[25] J.K. Lancaster, *Tribology Int., 23*(6) (1990) 371–379.
[26] M. Godet, *Wear, 100* (1984) 439–452.
[27] K. Hokkirigawa, *Wear, 151* (1991) 219–228.
[28] T. Fischer, *Ann. Rev. Mater. Sci., 18* (1988) 303–323.
[29] R. Silva and J. Vieira, *J. Hard Mater., 3*(1) (1992) 63–72.
[30] A.G. Evans and T.R. Wilshaw, *Acta. Metall., 24* (1976) 939–956.
[31] S.T. Buljan, S.F. Wayne and M.L. Huckabee, *J. Hard Mater., 3*(3–4) (1992) 379–391.